PLANETARY SCIENCE

Probing the hydrothermal system of the Chicxulub impact crater

David A. Kring[1]*, Sonia M. Tikoo[2], Martin Schmieder[1], Ulrich Riller[3], Mario Rebolledo-Vieyra[4], Sarah L. Simpson[5], Gordon R. Osinski[5], Jérôme Gattacceca[6], Axel Wittmann[7], Christina M. Verhagen[2], Charles S. Cockell[8], Marco J. L. Coolen[9], Fred J. Longstaffe[5], Sean P. S. Gulick[10], Joanna V. Morgan[11], Timothy J. Bralower[12], Elise Chenot[13], Gail L. Christeson[10], Philippe Claeys[14], Ludovic Ferrière[15], Catalina Gebhardt[16], Kazuhisa Goto[17], Sophie L. Green[18], Heather Jones[12], Johanna Lofi[19], Christopher M. Lowery[10], Rubén Ocampo-Torres[20], Ligia Perez-Cruz[21], Annemarie E. Pickersgill[22], Michael H. Poelchau[23], Auriol S. P. Rae[11,23], Cornelia Rasmussen[10,24], Honami Sato[25], Jan Smit[26], Naotaka Tomioka[27], Jaime Urrutia-Fucugauchi[21], Michael T. Whalen[28], Long Xiao[29], Kosei E. Yamaguchi[30]

The ~180-km-diameter Chicxulub peak-ring crater and ~240-km multiring basin, produced by the impact that terminated the Cretaceous, is the largest remaining intact impact basin on Earth. International Ocean Discovery Program (IODP) and International Continental Scientific Drilling Program (ICDP) Expedition 364 drilled to a depth of 1335 m below the sea floor into the peak ring, providing a unique opportunity to study the thermal and chemical modification of Earth's crust caused by the impact. The recovered core shows the crater hosted a spatially extensive hydrothermal system that chemically and mineralogically modified $\sim 1.4 \times 10^5$ km^3 of Earth's crust, a volume more than nine times that of the Yellowstone Caldera system. Initially, high temperatures of 300° to 400°C and an independent geomagnetic polarity clock indicate the hydrothermal system was long lived, in excess of 10^6 years.

INTRODUCTION

The Chicxulub impact crater, the largest surviving terrestrial impact basin with an uplifted peak ring (*1*), is well known for its link to the largest extinction event of the past 200 million years (*2–7*). A growing amount of attention is being directed at the crater's subsurface where impact heating and deformation generated a porous and permeable structure across the entire basin that was an ideal host for a hydrothermal system. Chemical and mineral alteration in the Chicxulub crater was previously detected within a few centimeter-size rock fragments from a petroleum exploration borehole (*3*) and an ~100-m-thick impactite sequence in the annular crater trough between the peak-ring and crater rim (*8–12*). On the basis of those limited data, a thermal model of the system was developed (Fig. 1)

(*13*) that suggested initially high temperatures (>300°C) within the peak-ring and crater-wide hydrothermal activity for 1.5 to 2.3 Ma adjacent to, and above, an ~3-km-thick cooling impact melt sheet (*14*). Testing this model was a key objective of offshore borehole M0077A drilled by International Ocean Discovery Program (IODP) and International Continental Scientific Drilling Program (ICDP) Expedition 364 (*15*). The project recovered hydrothermally altered impactites from a depth of 617 to 1335 m below the sea floor (mbsf), consisting of 130 m of impact melt rock and impact melt-bearing breccias overlying 588 m of shocked granitoid rocks and other crystalline target lithologies with impact-generated horizons of melt that were emplaced (*16*) during the late stages of peak-ring formation (*1, 17*). Impact melt-bearing breccias within the sequence (*15*) are

[1]Lunar and Planetary Institute, Universities Space Research Association, 3600 Bay Area Boulevard, Houston, TX 77058, USA. [2]Department of Earth and Planetary Sciences, Rutgers University New Brunswick, Piscataway Township, NJ 08854, USA. [3]Institut für Geologie, Universität Hamburg, Bundesstraße 55, 20146 Hamburg, Germany. [4]Departamento de Recursos del Mar, CINVESTAV-MÉRIDA, Carret. Merida-Progreso, S/N, Merida, Yucatán 97215, México. [5]Institute for Earth and Space Exploration and Department of Earth Sciences, The University of Western Ontario, London, ON N6A 5B7, Canada. [6]Aix Marseille Université, CNRS, Institut pour la Recherche et le Développement, Coll France, INRA, CEREGE, Aix-en-Provence, France. [7]Eyring Materials Center, Arizona State University, Tempe, AZ 85287-8301, USA. [8]Centre for Astrobiology, School of Physics and Astronomy, University of Edinburgh, Edinburgh EH9 3FD, UK. [9]School of Earth and Planetary Sciences, WA-Organic and Isotope Geochemistry Centre (WA-OIGC), Curtin University, Bentley, WA 6102, Australia. [10]Institute for Geophysics, Jackson School of Geosciences, University of Texas at Austin, Austin, TX 78758-4445, USA. [11]Department of Earth Science and Engineering, Imperial College London, London, SW7 2AZ, UK. [12]Department of Geosciences, Pennsylvania State University, University Park, PA 16802, USA. [13]GeoRessources, Université de Lorraine, CNRS, 54 500 Vandoeuvre-lès-Nancy, France. [14]Analytical, Environmental and Geo-Chemistry, Vrije Universiteit Brussel, Pleinlaan 2, Brussels 1050, Belgium. [15]Natural History Museum, Burgring 7, 1010 Vienna, Austria. [16]Alfred Wegener Institute Helmholtz Centre of Polar and Marine Research, 27568 Bremerhaven, Germany. [17]Department of Earth and Planetary Science, The University of Tokyo, Hongo 7-3-1, Tokyo 113-0033, Japan. [18]British Geological Survey, Edinburgh, UK. [19]Géosciences Montpellier, Université de Montpellier, 34095 Montpellier Cedex 05, France. [20]Groupe de Physico-Chimie de l'Atmosphère, L'Institut de Chimie et Procédés pour l'Énergie, l'Environnement et la Santé (ICPEES), UMR 7515 Université de Strasbourg–CNRS 1 rue Blessig, 67000 Strasbourg, France. [21]Instituto de Geofísica, Universidad Nacional Autónoma de México, Cd. Universitaria, Coyoacán, Ciudad de México C. P. 04510, México. [22]School of Geographical and Earth Sciences, University of Glasgow, Gregory, Lilybank Gardens, Glasgow G12 8QQ, UK. [23]University of Freiburg, Geology, Albertstraße 23b, 79104 Freiburg, Germany. [24]Department of Geology and Geophysics, University of Utah, 115 S 1460 E (FASB), Salt Lake City, UT 84112, USA. [25]Ocean Resources Research Center for Next Generation, Chiba Institute of Technology, 2-17-1, Tsudanuma, Narashino-city, Chiba 275-0016, Japan. [26]Faculty of Earth and Life Sciences (FALW), Vrije Universiteit Amsterdam, de Boelelaan 1085, Amsterdam 1018HV, Netherlands. [27]Kochi Institute for Core Sample Research, Japan Agency for Marine-Earth Science and Technology, 200 Monobe Otsu, Nankoku, Kochi 783-8502, Japan. [28]Department of Geosciences, University of Alaska Fairbanks, 1930 Yukon Drive, Fairbanks, AK 99775, USA. [29]China University of Geosciences (Wuhan), School of Earth Sciences, Planetary Science Institute, 388 Lumo Rd. Hongshan Dist., Wuhan, China. [30]Department of Chemistry, Toho University, Funabashi, Chiba 274-8510, Japan.
*Corresponding author. Email: kring@lpi.usra.edu
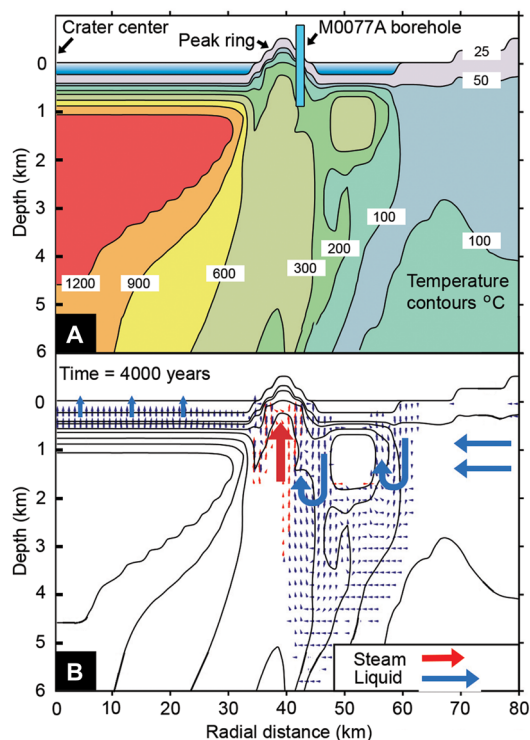
Fig. 1. Spatial context of hydrothermal system. Chicxulub hydrothermal evolution model (*12*) that was tested by Expedition 364 with a borehole into the peak ring ~40 km from the crater center. (**A**) Thermal contours of 25°, 50°, 100°, 200°, 300°, 600°, 900°, and 1200°C illustrate the location of the central melt pool (left side of diagram) and the thermal effect beneath the peak ring (middle of diagram). Temperature decreases with distance but is still ~300°C at the point corresponding to the base of the Expedition 364 borehole. (**B**) Water and steam flux vectors in the same region. Hydrothermal flow is particularly vigorous adjacent to the melt pool, in the vicinity of the peak ring. Water and steam do not penetrate the central melt pool until it has crystallized. Both panels represent the system 4000 years after impact. Full model details are available in (*13*). The ICDP Yaxcopoil-1 borehole, located on land, was drilled at a radial distance of ~65 km.

polymict breccias, containing clasts of variably shocked crystalline target rocks, sedimentary target rocks, and solidified impact melt, a lithology commonly called suevite.

RESULTS

Hydrothermal alteration was immediately evident in the core (Fig. 2), including permeable zones of bright red Na-dachiardite, heulandite, and analcime zeolites and dark green secondary clay accompanied by translucent-white calcite. After logging the core (supplementary materials text S1.1), we petrologically analyzed 68 splits to evaluate alteration assemblages and their paragenesis. In general, we found evidence for an initially hot (>300°C) hydrothermal system that subsequently cooled to produce a series of lower-temperature minerals.

Shatter cones, planar fractures (PFs), feather features (FFs), and planar deformation features (PDFs) in quartz, plus mineral transformations (e.g., TiO_2 to TiO_2-II; supplementary materials text S1.3) [(*1*, *15*) and this study] indicate peak shock pressures of ~15 to 20 GPa for the granitoid rocks. Such shock pressures imply postshock heating of ~170°C (*18*), with intervals of superheated (>1700°C) (*13*) impact melt that were produced by higher shock pressures, in rocks that
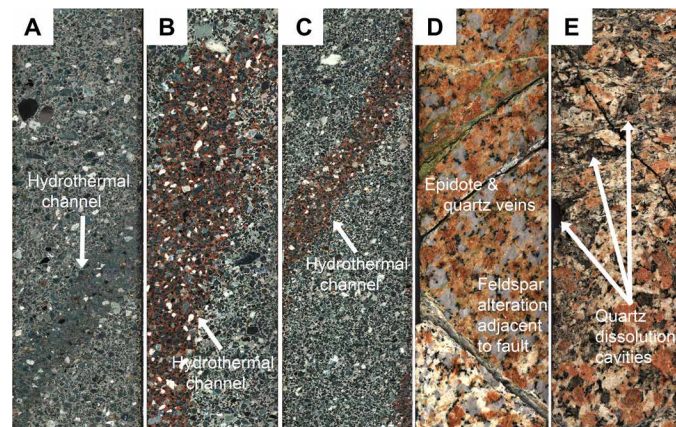

Fig. 2. Hydrothermally altered rock. Sawn surfaces through hydrothermally altered core samples, 83 mm wide. (**A**) Dark green porous, permeable channel that cuts through an impact melt-bearing breccia (suevite). The matrix of the breccia was dissolved before being partially replaced by secondary carbonate that grew from the fluid. Sample 007A-48R-3, 40 to 70 cm (643 mbsf). (**B** and **C**) Red-orange swath of Na-dachiardite and analcime cutting through impact melt-bearing breccia. The carbonate matrix of the breccia was dissolved in the hydrothermal channel, before Na-dachiardite, analcime, clay, and sparry calcite partially filled the channel. Samples 0077A-53R-3, 0 to 30 cm (658 mbsf), and 0077A-54R-1, 50 to 80 cm (660 mbsf). (**D**) Highly deformed, porous, and permeable peak-ring granitoid rock cut by a fault adjacent to altered feldspar and veins partly filled with quartz and epidote. Sample 0077A-129R-2, 0 to 30 cm (832 mbsf). (**E**) Granitoid rock with centimeter-size quartz dissolution cavities. Sample 0077A-275R-2, 0 to 30 cm (1248 mbsf).

had preimpact temperatures of ~185° to 255°C (supplementary materials text S1.10) at preimpact depths of 8 to 10 km (*1*).

Postimpact temperatures of ~355° to 425°C were maintained by heat from the adjacent ~3-km-thick central melt pool, inferred from scaling models (*13*) and consistent with a three-dimensional gravity model (*19*), long enough to facilitate a diverse suite of mineral alterations (Fig. 3) that crosscut shock deformation features in target rocks or overprint impact-generated melts and breccias and, therefore, must have occurred after the impact event. Calcium-Na and K-metasomatism, indicative of ≥300°C (*11*), are evident along the entire core. Impact melt rocks (in several intervals from ~721 to 747 and ~1207 to 1316 mbsf) with matrices of <10-μm-long laths of feldspar and Ca-pyroxene are also overprinted with alkali feldspar alteration fronts and crosscut by fractures with margins enriched in Ca-plagioclase. A K-feldspar–albite vein cuts across a granitoid rock at 887 mbsf.

Relict quartz from the target entrained in the melt rock (717 to 729 mbsf) has been partially to wholly dissolved, implying a hot, Si-undersaturated hydrothermal fluid. Deeper in the peak ring (1256 mbsf), adjacent to an interval of impact melt-bearing breccia, where the granitoid rock was deformed into a porous monomict breccia, the granitoid is honeycombed with quartz dissolution cavities (Fig. 2) that formed coincident with Ca-Na and K-metasomatism at temperatures of 300° to 400°C (*20*). Dissolution of quartz occurred intermittently elsewhere in the core, including quartz along PFs and silica glass along PDFs, increasing system porosity (fig. S3). In granitoid rock at 1085 mbsf, secondary muscovite crosscuts shock-metamorphic kinking of feldspar and, thus, formed postimpact at high zeolite or greenschist facies temperatures.

Hydrothermal andradite garnet ($Ca_3Fe^{3+}_2Si_3O_{12}$) precipitated in fluid-filled cavities within impact melt and granitoid rocks below
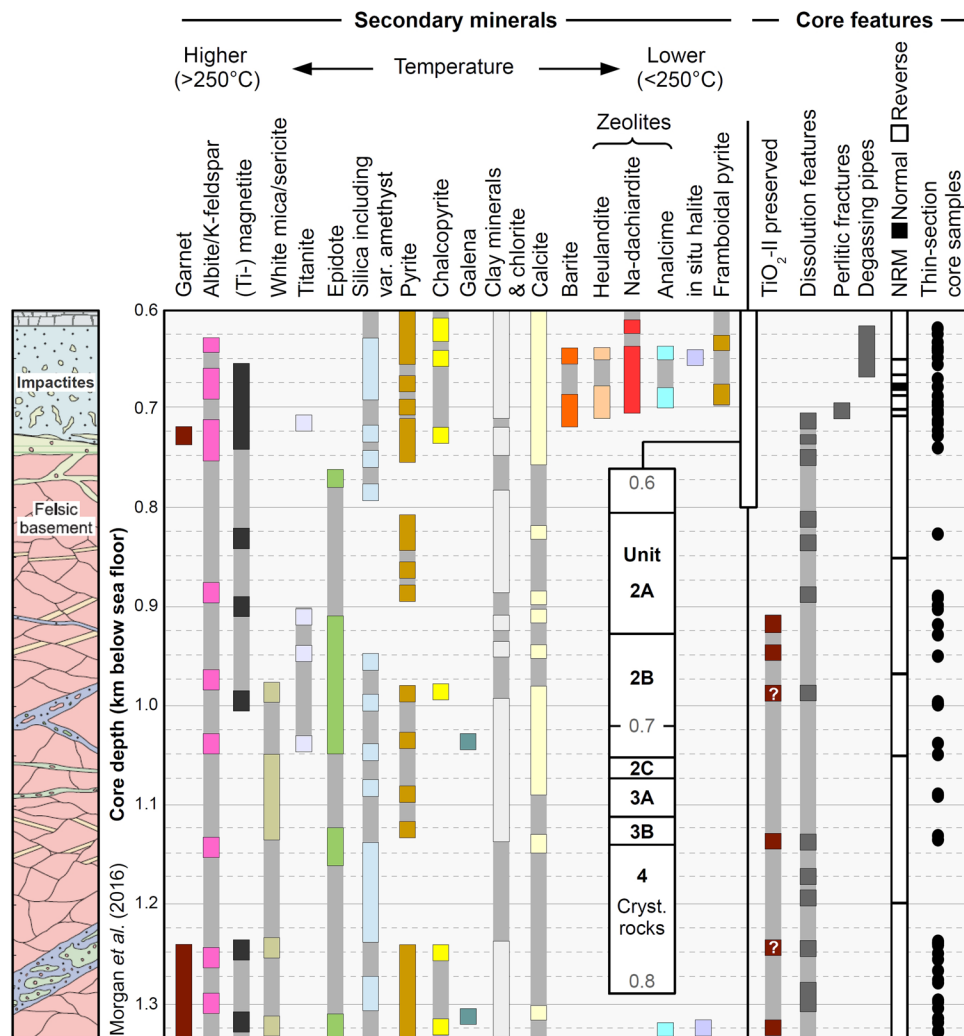
Fig. 3. Hydrothermal alteration with depth. Range chart with postimpact hydrothermal minerals correlated with core lithologies (15) and physical properties in the Chicxulub peak ring as measured in Expedition 364 Site 0077A core. The uppermost units of impact melt-bearing breccia (suevite) and impact melt rock between 617 and 747 mbsf were subdivided by the expedition (15) into units 2A, 2B, 2C, 3A, and 3B, which are shown in an inset beneath the ranges of low-temperature minerals. Garnet is andradite-grossular in the upper core section and mainly andradite in the lower core section. Natural remanent magnetization (NRM) of core samples shows both reverse and normal polarity.

1240 mbsf (Fig. 3) also implies ≳300°C (21). Hydrothermal garnet was also detected in an impact melt-bearing breccia near the top of the core (~730 mbsf), where it has Ti-rich crystal centers (replacing some of the Si) and grossular-rich rims (with Al replacing Fe^{3+}), reflecting temporally evolving hydrothermal fluid chemistry. Hydrothermal garnet was previously observed, albeit rarely, in samples from another drill core from the Chicxulub crater (ICDP Yaxcopoil-1) (21).

Preservation of shock-produced TiO_2-II (preliminary unofficial name) suggests maximum hydrothermal temperatures of 300° to 400°C, because this polymorph becomes increasingly unstable above 340°C and reverts to rutile within weeks above 440°C and minutes to hours above 500°C (22, 23).

As the system cooled to ≤300°C (11), a variety of Mg-Fe and Na-K sheet silicates precipitated. Melt fragments in the breccias were altered to smectite group minerals with chemical zoning and variable nH_2O (supplementary materials table S1 and text S1.4). Titanium-rich

biotite in granitoid rock was replaced by chlorite in the presence of epidote. Where a 2-cm-wide altered and microcrystalline melt vein cuts through granitoid rock at 1039 mbsf, the melt rock is enriched in Mg and K relative to the granitoid rock and contains distributed particles of Fe-sulfide. The granitoid rock, with albite ($An_1Ab_{97}Or_2$), K-feldspar ($An_1Ab_4Or_{95}$), and quartz, is crosscut with veins consisting of quartz, epidote, muscovite, a mafic aluminosilicate, and calcite with titanite and galena. Isolated precipitates of galena are associated with chalcopyrite in impact-generated fracture pore spaces.

Cavities, particularly in the polymict breccias (e.g., 685 mbsf) and impact melt rock (e.g., 730, 1301, and 1314 mbsf), are filled with secondary silica, epidote, calcite, barite, pyrite locally enriched in Co and Ni (bravoite), chalcopyrite, and coexisting analcime and Na-dachiardite (Fig. 4), sometimes with heulandite. The paragenesis of dachiardite is still poorly understood but has been produced experimentally at 250°C (24). Analcime can be produced from albite and water when temperatures cool below 200°C (25).
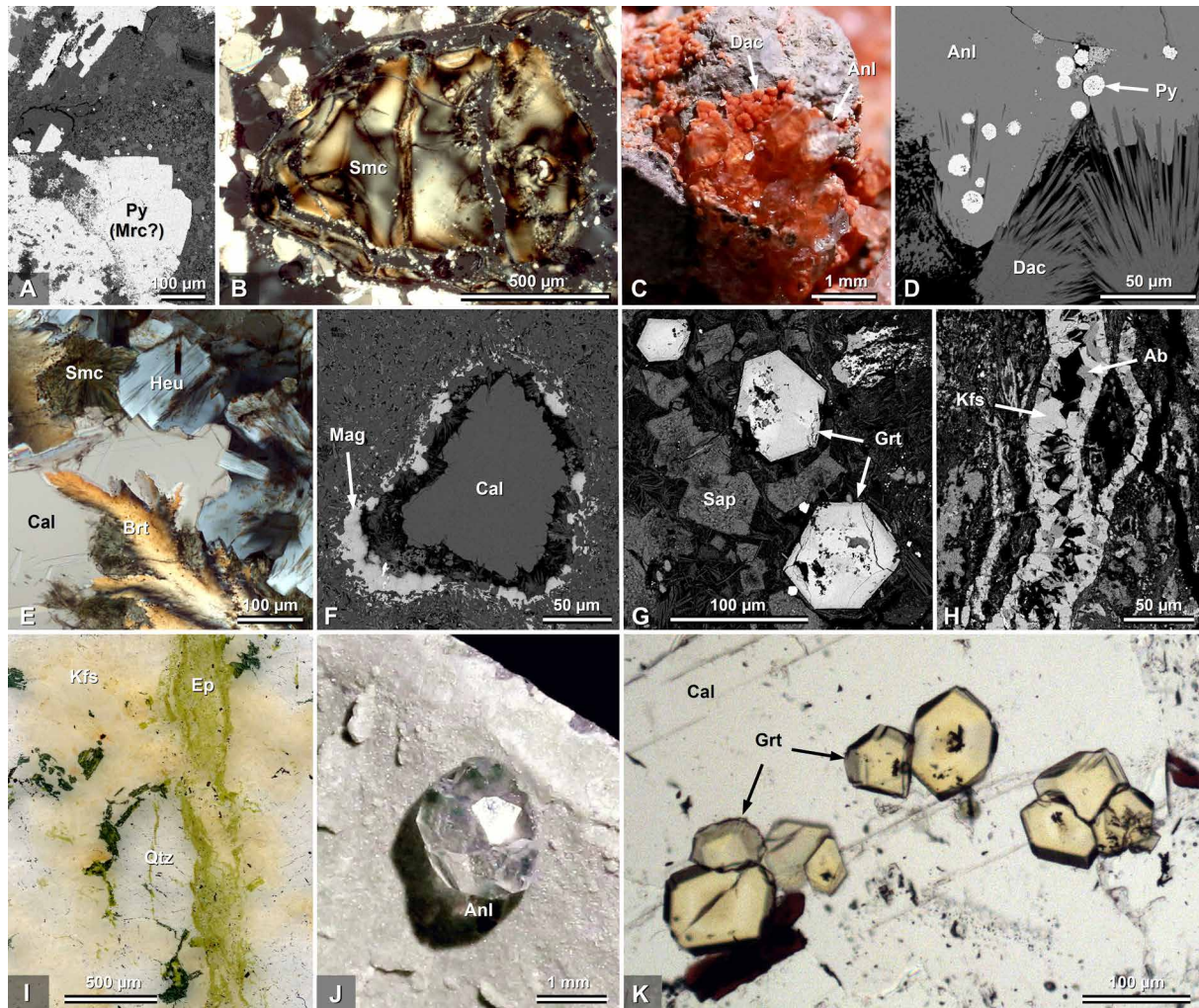
Fig. 4. Hydrothermal mineralization. (**A** to **K**) Hand specimen (C and J), optical microscopic (B, E, I, and K), and backscattered electron images (A, D, F, G, and H) of hydrothermal alteration minerals in the Chicxulub peak ring, presented in order of increasing depth. (A) Domain of euhedral FeS_2, either pyrite (Py), and/or the alternative dimorphic structure marcasite (Mrc), in suevite sample 0077A-40R-2, 105 to 107 cm (619 mbsf). (B) Impact glass fragment altered to montmorillonite-like sheet silicate in suevite sample 0077A-41R-1, 58 to 60 cm (638 mbsf). (C) Red Na-dachiardite (Dac) and transparent analcime (Anl) in suevite sample 0077A-60R-1, 90 to 92 cm (678 mbsf). (D) Framboidal pyrite (Py) associated with zeolite (analcime and Na-dachiardite) in suevite sample 0077A-63R-2, 69.5 to 72 cm (685 mbsf). (E) Sheaf-like barite (Brt) associated with zeolite (heulandite; Heu), smectite, and calcite (Cal) in suevite sample 0077A-71R-1, 55.5 to 57 cm (697 mbsf). (F) Secondary magnetite (Mag) surrounding a clay-lined vesicle filled with calcite in impact melt rock sample 0077A-85R-1, 26 to 28 cm (717 mbsf). (G) Zoned euhedral andradite-grossular garnet (Grt) crystals in mafic sheet silicate alteration domain, impact melt breccia sample 0077A-89R-3, 39 to 43 cm (729 mbsf). (H) Vein of albite (Ab) and K-feldspar (Kfs) crosscutting shocked basement granitoid sample 0077A-150R-3, 25.5 to 27 cm (887 mbsf). (I) Green epidote (Ep) vein crosscutting shocked granitoid sample 0077A-155R-1, 12 to 14 cm (897 mbsf). (J) Euhedral analcime crystal along open fracture in impact melt breccia sample 007A-293R-1, 10 to 12 cm (1301 mbsf). (K) Euhedral andradite garnet crystals in postimpact calcite (Cal) vein, impact melt breccia sample 0077A-299R-2, 10 to 12.5 cm (1321 mbsf). Photo credit for (C) and (J): M.S., LPI.

The low-temperature hydrothermal minerals (e.g., the zeolites analcime, heulandite, and Na-dachiardite) are concentrated in the uppermost ~130-m-thick portion of the core (Fig. 3), composed of impact melt-bearing breccias and impact melt rock. However, both of those units initially experienced a higher-temperature phase, as recorded by the growth of hydrothermal garnet.

Venting at the top of the postimpact hydrothermal system is implied by vertical alteration channels and partially to wholly filled pockets with sparry calcite and/or clay in the uppermost melt-bearing breccias between 617 and 623 mbsf (figs. S4 and S5). Similar features, albeit less well defined, were noted while logging core from ~626 to 636 mbsf. The sparry calcite shows strong local Mn zoning,

with some domains containing >2 weight % MnO (supplementary materials table S1). We also observe an increase in Mn abundances (Fig. 5) in the core interval that corresponds to the transition unit between peak-ring lithologies and crater-filling sediments. Manganese abundances in an x-ray fluorescence (XRF) core scan of the transition unit exceed that of the underlying suevite and seem to be unique features of the postimpact sediment-seawater interface. That may be due to hydrothermal venting of Mn. In complementary powder XRF data (Fig. 5), a more modest Mn anomaly occurs in the underlying bounding suevite and persists into the overlying carbonate sequence. If the Mn in the basal carbonate is also reflective of hydrothermal venting, then hydrothermal activity extended about 2.1 Ma
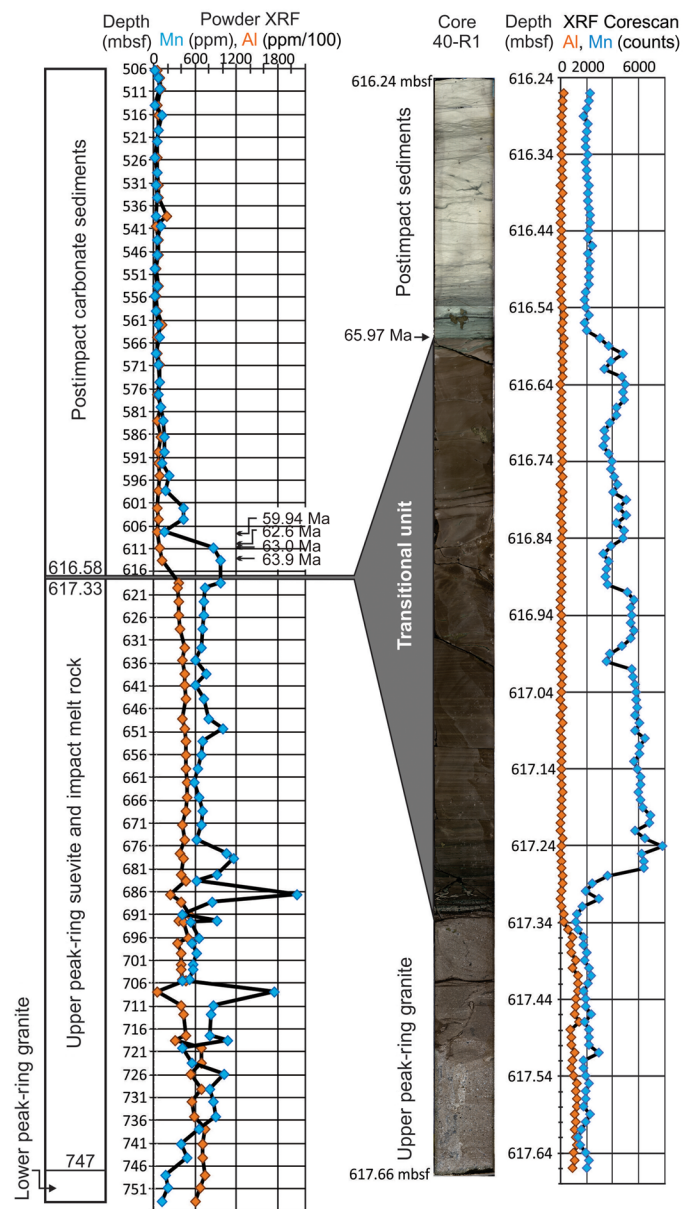
Fig. 5. Manganese anomaly. Manganese is strongly enriched in the transitional unit that is interpreted as sediment deposited in the immediate wake of the impact (*15*). Elevated concentrations of Mn were measured in samples beyond 2.1 Ma after the impact, based on correlated micropaleontologic data (*26*). Aluminum concentrations in these samples are shown as proxies for suevite components, suggesting the Mn anomalies in the transitional unit and the lowermost postimpact sediments are not correlated with reworked impactite debris.

into the postimpact carbonate sequence based on micropaleontology of those sediments (*26*). We recognize that [Mn] may reflect seafloor/pore water oxygenation and that, about 1.2 Ma after impact, there is evidence of increasing dysoxic conditions based on our expedition's study of biomarkers (*27*), but that activity is not coincident with the stratigraphic interval of [Mn] changes that we attribute to hydrothermal venting here.

Secondary sulfide minerals (pyrite, chalcopyrite, covellite, sphalerite, bravoite, and villamaninite) are common in the impact melt-bearing

breccias, sometimes intergrown with clausthalite, thorite, and Ni-rich pyrite aggregates that are similar to the Ni-rich pyrite associated with exhalative mineralization at the Sudbury impact structure (*28*). Pyrite framboids commonly coexist along open fractures filled with Na-dachiardite and analcime (Fig. 4) and along margins of vertical channels venting to the seafloor within the impact basin (fig. S4). While some of those channels have sparry calcite (fig. S4), others are filled with a porous assemblage of sheet silicates and accessory minerals. Pyrite framboids were observed to be concentrated along the margin of a pipe (fig. S5), where chemical gradients occurred between venting fluid and breccia wallrock.

As noted previously and shown in Fig. 4, these hydrothermal minerals and mineral assemblages crosscut shock deformation features of target rocks or overprint impact lithologies and, thus, are due to postimpact alteration. It is important to note that portions of the target rocks were altered before impact. There is, for example, an alteration halo in granitoid rock adjacent to dolerite intrusions that predates shock deformation. The preimpact alteration and its timing are being examined by other Expedition 364 team members and will be reported elsewhere in an analysis of intrusions and assembly of the Yucatán peninsula's Maya block.

The occurrence of primary and secondary (Ti-)magnetite grains in the upper peak ring suggests that paleomagnetic measurements (supplementary materials text S1.9) may elucidate whether the peak ring cooled within geomagnetic Chron 29r (which corresponds to the time of impact) or substantially later. We observed reversed polarity characteristic remanent magnetizations in impact melt rocks and an immediately overlying impact melt-bearing breccia unit that likely reflect thermoremanent magnetization acquired during primary cooling in Chron 29r. Higher in the peak ring, reversed polarity magnetizations are also observed within impact melt-bearing breccias, but zones exhibiting normal polarity exist as well (Fig. 3). These upper breccia units are interpreted to have formed as wash-back deposits following crater modification (*29*) and were, therefore, likely emplaced at temperatures far below the 580°C Curie temperature of magnetite, precluding full thermoremanent magnetization as the remanence mechanism. While it is possible that normal randomly oriented breccia clasts retained predepositional magnetization, we show that the distribution of magnetic inclinations observed for the upper peak-ring breccias is unlikely to entirely result from predepositional remanence (supplementary materials text S1.9). Therefore, magnetization in the upper breccia unit is most likely a chemical remanence from the formation of secondary (Ti-)magnetite during protracted hydrothermal activity extending into a normal polarity interval.

DISCUSSION

The Expedition 364 core shows the impact-induced hydrothermal system extended to a depth at least 700 m beneath the surface of the peak ring, far deeper than the ~100-m-thick unit of hydrothermal alteration observed (*8–12*) in the region between the peak ring and crater rim sampled by the Yaxcopoil-1 borehole. Hydrothermal fluids moved along fractures, cataclasite zones, and veins in each meter of core, sometimes with millimeter to centimeter spacing, in impact-deformed granitoid rock with a mean density that is about 10% lower than that of typical felsic basement rocks (*1*). Fluid flow also occurred along lithological boundaries, for example, between units of impact melt-bearing breccias and impact melt rock. Deeper in the core, alteration is more extensive at the contacts between melt zones and

granitoid rocks. Fluid flow was extensive, as secondary carbonate is pervasive and likely deposited by fluids that circulated through and dissolved portions of the preimpact carbonate sequence that occurs ~2 km beneath the bottom of the borehole [(30); see also (1) and Figure 5 of (31)].

Hydrothermal fluids were initially hot and Si undersaturated, but likely evolved as the system cooled and aged. Fluid chemistry was likely complex spatially, too. Near-neutral pH conditions are implied by the precipitation of quartz and pyrite, but increasingly alkaline conditions are implied by the precipitation of smectite, related phyllosilicates, and calcite. A system model (13) suggests water was dominantly groundwater in origin, rather than due to seawater drawdown, which is consistent with isotopic analyses of Yaxcopoil-1 core samples (32) located farther from the crater center. Those analyses suggested the fluid had high salinities (~20%) and minor kerogen contents that are consistent with a basinal hydrocarbon-bearing (or oil-field) saline brine that eventually, at lower temperatures [i.e., 75° to 100°C (10)], precipitated secondary sparry calcite. Although the system may have been dominated by groundwater, seawater influence, particularly at the top of the sequence, is still possible. Analyses of stable isotopes, fluid inclusions, and accessory mineral assemblages, such as those involving sulfur, will be needed in the recently acquired core to provide an integrated assessment of fluid chemistry as a function of time and depth in the core.

The hydrothermal system was long-lived because the mineral assemblages indicate >300°C initial temperatures that, in the thermal model (13), require ~2 Ma to cool to below 90°C within 1 km of the surface. This modeling constraint agrees with the observed 5.8-m-thick relative enrichment of Mn in the postimpact carbonate sediments that overlie the peak-ring suevite. This Mn enrichment suggests venting until at least 2.1 Ma after the impact at the drill site on top of Chicxulub's peak ring (Fig. 5). A similar Mn anomaly has been observed in the Yaxcopoil-1 drill core, where it extends at least 6.5 m into the postimpact carbonate sediments (12); its interpretation, however, was hampered by incomplete biostratigraphic data [cf. (33)]. At mid-ocean ridge vents, Mn is slow to oxidize in hydrothermal plumes compared with other dissolved elements. Therefore, Mn oxide particles are produced over longer time scales and occur in the distal part of vents (12, 34, 35). The lack of correlated relative enrichments in other elements possibly related to detrital input in the Mn-enriched postimpact carbonate sediments such as Al (Fig. 5) supports the interpretation of Mn as a proxy for prolonged hydrothermal venting in the Chicxulub impact crater.

Paleomagnetism may also be used to place temperature constraints in the upper peak ring. Normal polarity magnetization was measured in breccia samples from the Expedition 364 core as well as those from Yaxcopoil-1 (36). If these normal polarities reflect chemical remanent magnetization, the magnetic data suggest the hydrothermal system likely remained at or above ~100° to 250°C [i.e., a typical temperature used for hydrothermal synthesis of magnetite in laboratory settings (37)] for at least 150,000 years (and possibly as long as 500,000 years), the first time when normal polarity occurred after the impact (38), calculated using a recent high-precision argon isotopic age and 2σ error values (39). These temperatures are far higher than the ~50°C value predicted by the cooling model (13) at 200,000 years after the impact. It is, thus, possible that the thermal model (13) is too conservative and underestimates the lifetime of the system or did not resolve local excursions in postimpact temperatures and cooling rates on a scale of meters to tens of meters.

The analyses described here resolve several questions about impact-generated hydrothermal systems. The peak ring is deformed [see also (17, 40)] and, thus, permeable to fluid flow similar to model results (13). The peak ring is hydrothermally altered, confirming the impact-generated system was widespread across the Chicxulub impact basin. The system extended to depths of 5 to 6 km (13) and, thus, chemically and mineralogically altered $\sim 1.4 \times 10^5$ km^3 of Earth's crust (supplementary materials text S1.12). The Ca-Na-K metasomatism, quartz dissolution, and garnet precipitation indicate the system was sufficiently hot (c. 300° to 400°C) to have persisted for at least 2 Ma (13). An Mn signature of venting in overlying crater-filling sediments, likewise, suggests an active hydrothermal system for at least 2.1 Ma. Independent paleomagnetic signatures of normal polarity in the Fe-bearing hydrothermal minerals suggest a minimum system lifetime of 200,000 years at temperatures possibly above 250°C. Such temperatures so long after impact suggest conditions [~90° within 1 km of the surface (13)] to drive hydrothermal activity may have persisted >2 Ma.

Observations of an extensive hydrothermal system at Chicxulub imply similar systems once existed at the eroded ~250-km-diameter 2.02 Ga-old Vredefort structure and at the ~200-km-diameter 1.85 Ga-old Sudbury structure. The latter of which traces of hydrothermal activity (41) consistent with those observed here. Likewise, similar systems are implied in even larger impact craters, into continental and oceanic crust, inferred from ejecta horizons in 2.49 to 3.47 Ga-old Paleoproterozoic, Neoarchean, and Paleoarchean sections in South Africa and Western Australia (42, 43).

Drilling results demonstrate there were sufficient habitats for microorganisms within the peak ring of the Chicxulub impact crater. The hydrothermal system created a network of porous, permeable niches perfect for microbial ecosystems. Domains of pervasive clay mineral (smectite) alteration (e.g., at depths of 721 to 747 mbsf) with high surface-to-volume ratio and sharp chemical and physical gradients could provide one of several potential habitable volumes for microbial colonization. Sulfide framboids in several partially filled fractures, with biologically compatible low-temperature mineral assemblages, implying sulfate and sulfur reduction (e.g., SO_4^{2-} to H_2S, SO to H_2S, S^0 to H_2S), were viable energy sources for microorganisms. Coexistence of iron oxides with sulfides and andradite with saponite suggest Fe^{3+} to Fe^{2+} reduction is also a possible electron donor for biological systems, with redox gradients in the system allowing for iron oxidation elsewhere.

The paleomagnetic results suggest that cooling from initially high (~350°C) temperatures to those suitable for thermophilic and hyperthermophilic life (~50° to 120°C) likely took >10^5 years. This constraint, in conjunction with hydrothermal system evolution modeling (13), indicates habitable conditions existed in the middle to the upper part of the peak ring for 10^4 to 10^5 years or longer.

The extent and longevity of the hydrothermal system, therefore, support the impact origin of life hypothesis for the Hadean (44–46), when the entire surface of Earth was affected by ~6000 impactors larger than the ~10-km Chicxulub impactor [including ~5 larger than 500-km diameter and 3 larger than 700 km (47)]. Those impactors would have produced larger craters in the hotter Hadean lithosphere than they would today (48), including ~200 impact craters that are 1000 to 5000 km in diameter.

As with Chicxulub, zones with temperatures suitable for organisms in those basins would migrate inward as the basins cooled. If the sialic target lithologies at Chicxulub are a proxy for Hadean crust

as some propose (*49*) and is consistent with a possible Hadean rock fragment (*50*), then hydrothermal clays may have been a catalyst for RNA synthesis on the early Earth (*51*). Serpentinization and its energy sources for life (*52*) would have been the correlative hydrothermal alteration products when impacts occurred in mafic crust. Those environments can host several redox reactions (e.g., $S^0 + H_2 \rightarrow H_2S$; $CH_4 + SO_4^+ \rightarrow HS^- + HCO_3^- + H_2O$; $SO_4^{2-} + H^+ + 4H_2 \rightarrow HS^- + 4H_2O$) that are suitable energy sources for microbial systems, including hyperthermophilic archaea, thermophilic Deltaproteobacteria, and lower-temperature microbial mats (*53*). The porosity and permeability of the Hadean crust are unknown but may have been high due to the effects of impact bombardment, as implied by observations at Chicxulub (*54*) and as seen on the Moon, where impacts created 12% porosity in a crystalline crust of similar age to depths of at least a few kilometers and probably to the mantle (*55*).

The hydrothermally altered Expedition 364 core demonstrates that impact cratering is a fundamentally important heat engine in emerging planetary systems and that the geologically young Chicxulub crater is a suitable analog for terrestrial impact basins created almost 4 Ga ago. Impact-generated hydrothermal systems were prominent features on early Earth and wherever water exists in a planetary crust. This model is transferrable to an early Mars (e.g., *56–60*) and any exoplanetary system with similar conditions.

SUPPLEMENTARY MATERIALS

Supplementary material for this article is available at http://advances.sciencemag.org/cgi/content/full/6/22/eaaz3053/DC1

REFERENCES AND NOTES

1. J. V. Morgan, S. P. S. Gulick, T. Bralower, E. Chenot, G. Christeson, P. Claeys, C. Cockell, G. S. Collins, M. J. L. Coolen, L. Ferrière, C. Gebhardt, K. Goto, H. Jones, D. A. Kring, E. le Ber, J. Lofi, X. Long, C. Lowery, C. Mellett, R. Ocampo-Torres, G. R. Osinski, L. Perez-Cruz, A. Pickersgill, M. Poelchau, A. Rae, C. Rasmussen, M. Rebolledo-Vieyra, U. Riller, H. Sato, D. R. Schmitt, J. Smit, S. Tikoo, N. Tomioka, J. Urrutia-Fucugauchi, M. Whalen, A. Wittmann, K. E. Yamaguchi, W. Zylberman, The formation of peak rings in large impact craters. *Science* **354**, 878–882 (2016).
2. A. R. Hildebrand, G. T. Penfield, D. A. Kring, M. Pilkington, A. Camargo Z, S. B. Jacobsen, W. V. Boynton, Chicxulub Crater: A possible Cretaceous/Tertiary boundary impact crater on the Yucatán Peninsula, Mexico. *Geology* **19**, 867–871 (1991).
3. D. A. Kring, W. V. Boynton, Petrogenesis of an augite-bearing melt rock in the Chicxulub structure and its relationship to K/T impact spherules in Haiti. *Nature* **358**, 141–144 (1992).
4. C. C. Swisher III, J. M. Grajales-Nishimura, A. Montanari, S. V. Margolis, P. Claeys, W. Alvarez, P. Renne, E. Cedillo-Pardoa, F. J. Maurrasse, G. H. Curtis, J. Smit, M. O. McWilliams, Coeval $^{40}Ar/^{39}Ar$ ages of 65.0 million years ago from Chicxulub crater melt rock and Cretaceous-Tertiary boundary tektites. *Science* **257**, 954–958 (1992).
5. J. Smit, The global stratigraphy of the cretaceous-tertiary boundary impact ejecta. *Annu. Rev. Earth Planet. Sci.* **27**, 75–113 (1999).
6. D. A. Kring, The Chicxulub impact event and its environmental consequences at the Cretaceous–Tertiary boundary. *Palaeogeogr. Palaeoclim. Palaeocol.* **255**, 4–21 (2007).
7. P. Schulte, L. Alegret, I. Arenillas, J. A. Arz, P. J. Barton, P. R. Bown, T. J. Bralower, G. L. Christeson, P. Claeys, C. S. Cockell, G. S. Collins, A. Deutsch, T. J. Goldin, K. Goto, J. M. Grajales-Nishimura, R. A. F. Grieve, S. P. S. Gulick, K. R. Johnson, W. Kiessling, C. Koeberl, D. A. Kring, K. G. MacLeod, T. Matsui, J. Melosh, A. Montanari, J. V. Morgan, C. R. Neal, D. J. Nichols, R. D. Norris, E. Pierazzo, G. Ravizza, M. Rebolledo-Vieyra, W. U. Reimold, E. Robin, T. Salge, R. P. Speijer, A. R. Sweet, J. Urrutia-Fucugauchi, V. Vajda, M. T. Whalen, P. S. Willumsen, The chicxulub asteroid impact and mass extinction at the cretaceous-paleogene boundary. *Science* **327**, 1214–1218 (2010).
8. D. E. Ames, I. M. Kjarsgaard, K. O. Pope, B. Dressler, M. Pilkington, Secondary alteration of the impactite and mineralization in the basal Tertiary sequence, Yaxcopoil-1, Chicxulub impact crater, Mexico. *Meteoritics Planet. Sci.* **39**, 1145–1167 (2004).
9. L. Hecht, A. Wittmann, R.-T. Schmitt, D. Stöffler, Composition of impact melt particles and the effects of post-impact alteration in suevitic rocks at the Yaxcopoil-1 drill core, Chicxulub crater, Mexico. *Meteoritics Planet. Sci.* **39**, 1169–1186 (2004).
10. V. Lüders, K. Rickers, Fluid inclusion evidence for impact-related hydrothermal fluid and hydrocarbon migration in Creataceous sediments of the ICDP-Chicxulub drill core Yax-1. *Meteoritics Planet. Sci.* **39**, 1187–1197 (2004).
11. L. Zürcher, D. A. Kring, Hydrothermal alteration in the core of the Yaxcopoil-1 borehole, Chicxulub impact structure, Mexico. *Meteoritics Planet. Sci.* **39**, 1199–1221 (2004).
12. A. J. Rowe, J. J. Wilkinson, B. J. Coles, J. V. Morgan, Chicxulub: Testing for post-impact hydrothermal input into the Tertiary ocean. *Meteoritics Planet. Sci.* **39**, 1223–1231 (2004).
13. O. Abramov, D. A. Kring, Numerical modeling of impact-induced hydrothermal activity at the Chicxulub crater. *Meteoritics Planet. Sci.* **42**, 93–112 (2007).
14. D. A. Kring, Hypervelocity collisions into continental crust composed of sediments and an underlying crystalline basement: Comparing the Ries (~24 km) and Chicxulub (~180 km) impact craters. *Geochemistry* **65**, 1–46 (2005).
15. J. Morgan, S. Gulick, C. L. Mellett, S. L. Green, The Expedition 364 Scientists, Chicxulub: Drilling the K-Pg Impact Crater, Proceedings of the International Ocean Discovery Program (College Station, TX (International Ocean Discovery Program), 2017), vol. 364.
16. D. A. Kring, M. Schmieder, B. J. Shaulis, U. Riller, C. Cockell, M. J. L. Coolen, and the IODP-ICDP Expedition 364 Science Party, Probing the impact-generated hydrothermal system in the peak ring of the Chicxulub crater and its potential as a habitat. *Lunar Planet. Sci. XLVIII*, Abstract #1212 (2017).
17. U. Riller, M. Poelchau, A. S. P. Rae, F. M. Schulte, G. S. Collins, J. Melosh, R. A. F. Grieve, J. V. Morgan, S. P. S. Gulick, J. Lofi, A. Diaw, N. M. Call, D. A. Kring; The IODP-ICDP Expedition 364 Science Party, Rock fluidization during peak-ring formation of large impact structures. *Nature* **562**, 511–518 (2018).
18. D. Stöffler, C. Hamann, K. Metzler, Shock metamorphism of planetary silicate rocks and sediments: Proposal for an updated classification system. *Meteoritics Planet. Sci.* **53**, 5–49 (2018).
19. J. Ebbing, P. Janle, J. Koulouris, B. Milkereit, 3D gravity modelling of the Chicxulub impact structure. *Planetary Space Sci.* **49**, 599–609 (2001).
20. M. Cathelineau, The hydrothermal alkali metasomatism effects on granitic rocks: Quartz dissolution and related subsolidus changes. *J. Petrol.* **27**, 945–965 (1986).
21. M. J. Nelson, H. E. Newsom, M. N. Spilde, T. Salge, Petrographic investigation of melt and matrix relationships in Chicxulub crater Yaxcopoil-1 brecciated melt rock and melt rock-bearing suevite (846–885m, units 4 and 5). *Geochim. Cosmochim. Acta* **86**, 1–20 (2012).
22. R. G. McQueen, J. C. Jamieson, S. P. Marsh, Shock-wave compression and x-ray studies of titanium dioxide. *Science* **155**, 1401–1404 (1967).
23. R. K. Linde, P. S. DeCarli, Polymorphic behavior of titania under dynamic loading. *J. Chem. Phys.* **50**, 319–325 (1969).
24. K. G. Knauss, Lawrence Livermore National Laboratory Publ. No. UCRL-53645 (1985).
25. J. G. Liou, Analcime equilibria. *Lithos* **4**, 389–402 (1971).
26. C. M. Lowery, T. J. Bralower, J. D. Owens, F. J. Rodríguez-Tovar, H. Jones, J. Smit, M. T. Whalen, P. Claeys, K. Farley, S. P. S. Gulick, J. V. Morgan, S. Green, E. Chenot, G. L. Christeson, C. S. Cockell, M. J. L. Coolen, L. Ferrière, C. Gebhardt, K. Goto, D. A. Kring, J. Lofi, R. Ocampo-Torres, L. Perez-Cruz, A. E. Pickersgill, M. H. Poelchau, A. S. P. Rae, C. Rasmussen, M. Rebolledo-Vieyra, U. Riller, H. Sato, S. M. Tikoo, N. Tomioka, J. Urrutia-Fucugauchi, J. Vellekoop, A. Wittmann, L. Xiao, K. E. Yamaguchi, W. Zylberman, Rapid recovery of life at ground zero of the end-Cretaceous mass extinction. *Nature* **558**, 288–291 (2018).
27. B. Schaefer, K. Grice, M. J. L. Coolen, R. E. Summons, X. Cui, T. Bauersachs, L. Schwark, M. E. Böttcher, T. J. Bralower, S. L. Lyons, K. H. Freeman, C. S. Cockell, S. P. S. Gulick, J. V. Morgan, M. T. Whalen, C. M. Lowery, V. Vajda, Microbial life in the nascent Chicxulub crater. *Geology* **48**, 328–332 (2020).
28. G. A. Desborough, R. R. Larson, Nickel-bearing iron sulfides in the Onaping Formation, Sudbury Basin, Ontario. *Econ. Geol.* **65**, 728–730 (1970).
29. S. P. S. Gulick, T. J. Bralower, J Ormö, B. Hall, K. Grice, B. Schaefer, S. Lyons, K. H. Freeman, J. V. Morgan, N. Artemieva, P. Kaskes, S. J. de Graaff, M. T. Whalen, G. S. Collins, S. M. Tikoo, C. Verhagen, G. L. Christeson, P. Claeys, M. J. L. Coolen, S. Goderis, K. Goto, R. A. F. Grieve, N. McCall, G. R. Osinski, A. S. P. Rae, U. Riller, J. Smit, V. Vajda, A. Wittmann, The Expedition 364 Scientists, The first day of the Cenozoic. *Proc. Natl. Acad. Sci. U.S.A.* **116**, 19342–19351 (2019).
30. S. P. S. Gulick, G. L. Christeson, P. J. Barton, R. A. F. Grieve, J. V. Morgan, J. Urrutia-Fucugauchi, Geophysical characterization of the Chicxulub impact crater. *Rev. Geophys.* **51**, 31–52 (2013).
31. D. A. Kring, P. Claeys, S. P. S. Gulick, J. V. Morgan, G. S. Collins, The IODP-ICDP Expedition Science Party, Chicxulub and the exploration of large peak-ring impact craters through scientific drilling. *GSA Today* **27**, 4–8 (2017).
32. L. Zurcher, D. A. Kring, M. D. Barton, D. Dettman, M. Rollog, Stable isotope record of post-impact fluid activity in the core of the Yaxcopoil-1 borehole, Chicxulub impact structure, Mexico *Special Paper of the Geological Society of America* (2005), vol. 384, pp. 223–238.
33. J. A. Arz, L. Alegret, I. Arenillas, Foraminiferal biostratigraphy and paleoenvironmental reconstruction at the Yaxcopoil-1 drill hole, Chicxulub crater, Yucatán Peninsula. *Meteoritics Planet. Sci.* **39**, 1099–1111 (2004).

34. M. J. Mottl, T. F. McConachy, Chemical processes in buoyant hydrothermal plumes on the East Pacific Rise near 21°N. *Geochim. Cosmochim. Acta* **54**, 1911–1927 (1990).

35. M. J. Mottl, F. J. Sansone, C. Geoffrey Wheat, J. A. Resing, E. T. Baker, J. E. Lupton, Manganese and methane in hydrothermal plumes along the East Pacific Rise, 8°40′ to 11°50′N. *Geochim. Cosmochim. Acta* **59**, 4147–4165 (1995).

36. M. Rebolledo-Vieyra, J. Urrutia-Fucugauchi, Magnetostratigraphy of the impact breccias and post-impact carbonates from borehole Yaxcopoil-1, Chicxulub impact crater, Yucatán, Mexico. *Meteoritics Planet. Sci.* **39**, 821–829 (2004).

37. M. N. Viswanathiah, J. A. K. Tareen, K. V. Krishnamurthy, Low temperature hydrothermal synthesis of magnetite. *J. Cryst. Growth* **49**, 189–192 (1980).

38. W. C. Clyde, J. Ramezani, K. R. Johnson, S. A. Bowring, M. M. Jones, Direct high-precision U–Pb geochronology of the end-Cretaceous extinction and calibration of Paleocene astronomical timescales. *Earth Planet. Sci. Lett.* **452**, 272–280 (2016).

39. C. J. Sprain, P. R. Renne, W. A. Clemens, G. P. Wilson, Calibration of chron C29r: New high-precision geochronologic and paleomagnetic constraints from the Hell Creek region, Montana. *GSA Bulletin* **130**, 1615–1644 (2018).

40. A. S. P. Rae, G. S. Collins, J. V. Morgan, T. Salge, G. L. Christeson, J. Leung, J. Lofi, S. P. S. Gulick, M. Poelchau, U. Riller, C. Gebhardt, R. A. F. Grieve, G. R. Osinski, The IODP-ICDP Expedition 364 Scientists, Impact-induced porosity and microfracturing at the Chicxulub impact structure. *J. Geophys. Res. Planets* **124**, 1960–1978 (2019).

41. D. E. Ames, I. R. Jonasson, H. L. Gibson, K. O. Pope, in *Biological Processes Associated with Impact Events* (Springer-Verlag, 2006), pp. 55–100.

42. B. Rasmussen, T. S. Blake, I. R. Fletcher, U-Pb zircon age constraints on the Hamersley spherule beds: Evidence for a single 2.63 Ga Jeerinah-Carawine impact ejecta layer. *Geology* **33**, 725–728 (2005).

43. A. E. Krull-Davatzes, G. R. Byerly, D. R. Lowe, Paleoarchean ocean crust and mantle excavated by meteor impact: Insight into early crustal processes and tectonics. *Geology* **42**, 635–638 (2014).

44. D. A. Kring, Impact events and their effect on the origin, evolution, and distribution of life. *GSA Today* **10**, 1–7 (2000).

45. D. A. Kring, *The First Billion Years – Habitability*, Abstract #1037 (2019).

46. D. A. Kring, Environmental consequences of impact cratering events as a function of ambient conditions on Earth. *Astrobiology* **3**, 133–152 (2003).

47. S. Marchi, W. F. Bottke, L. T. Elkins-Tanton, M. Bierhaus, K. Wuennemann, A. Morbidelli, D. A. Kring, Widespread mixing and burial of Earth's Hadean crust by asteroid impacts. *Nature* **511**, 578–582 (2014).

48. R. W. K. Potter, D. A. Kring, G. S. Collins, Scaling of basin-sized impacts and the influence of target temperature, in *Large Meteorite Impacts and Planetary Evolution V*, G. R. Osinski, D. A. Kring, Eds. (Geological Society of America, Boulder, 2015), pp. 99–113.

49. T. M. Harrison, M. M. Wielicki, From the Hadean to the Himalaya: 4.4 Ga of felsic terrestrial magmatism. *Am. Mineral.* **101**, 1348–1359 (2016).

50. J. J. Bellucci, A. A. Nemchin, M. Grange, K. L. Robinson, G. Collins, M. J. Whitehouse, J. F. Snape, M. D. Norman, D. A. Kring, Terrestrial-like zircon in a clast from an Apollo 14 breccia. *Earth Planet. Sci. Lett.* **510**, 173–185 (2019).

51. J. P. Ferris, Mineral catalysis and prebiotic synthesis: Montmorillonite-catalyzed formation of RNA. *Elements* **1**, 145–149 (2005).

52. M. J. Russell, A. J. Hall, W. Martin, Serpentinization as a source of energy at the origin of life. *Geobiology* **8**, 355–371 (2010).

53. W. Martin, J. Baross, D. Kelley, M. J. Russell, Hydrothermal vents and the origin of life. *Nat. Rev. Microbiol.* **6**, 805–814 (2008).

54. G. L. Christeson, S. P. S. Gulick, J. V. Morgan, C. Gebhardt, D. A. Kring, E. le Ber, J. Lofi, C. Nixon, M. Poelchau, A. S. P. Rae, M. Rebolledo-Vieyra, U. Riller, D. R. Schmitt, A. Wittmann, T. J. Bralower, E. Chenot, P. Claeys, C. S. Cockell, M. J. L. Coolen, L. Ferrière, S. Green, K. Goto, H. Jones, C. M. Lowery, C. Mellett, R. Ocampo-Torres, L. Perez-Cruz, A. E. Pickersgill, C. Rasmussen, H. Sato, J. Smit, S. M. Tikoo, N. Tomioka, J. Urrutia-Fucugauchi, M. T. Whalen, L. Xiao, K. E. Yamaguchi, Extraordinary rocks from the peak ring of the Chicxulub impact crater: P-wave velocity, density, and porosity measurements from IODP/ICDP Expedition 364. *Earth Planet. Sci. Lett.* **495**, 1–11 (2018).

55. M. A. Wieczorek, G. A. Neumann, F. Nimmo, W. S. Kiefer, G. J. Taylor, H. J. Melosh, R. J. Phillips, S. C. Solomon, J. C. Andrews-Hanna, S. W. Asmar, A. S. Konopliv, F. G. Lemoine, D. E. Smith, M. M. Watkins, J. G. Williams, M. T. Zuber, The crust of the moon as seen by GRAIL. *Science* **339**, 671–675 (2013).

56. H. E. Newsom, J. J. Hagerty, I. E. Thorsos, Location and sampling of aqueous and hydrothermal deposits in Martian impact craters. *Astrobiology* **1**, 71–88 (2001).

57. J. A. Rathbun, S. W. Squyres, Hydrothermal systems associated with martian impact craters. *Icarus* **157**, 362–372 (2002).

58. O. Abramov, D. A. Kring, Impact-induced hydrothermal activity on early Mars. *J. Geophys. Res.* **110**, E12S09 (2005).

59. S. P. Schwenzer, D. A. Kring, Impact-generated hydrothermal systems capable of forming phyllosilicates on Noachian Mars. *Geology* **37**, 1091–1094 (2009).

60. G. R. Osinski, L. L. Tornabene, N. R. Banerjee, C. S. Cockell, R. Flemming, M. R. M. Izawa, J. M. Cutcheon, J. Parnell, L. J. Preston, A. E. Pickersgill, A. Pontefract, H. M. Sapers, G. Southam, Impact-generated hydrothermal systems on Earth and Mars. *Icarus* **224**, 347–363 (2012).

61. K. L. Thomas-Keprta, S. J. Clemett, S. Messenger, D. K. Ross, L. le, Z. Rahman, D. S. McKay, E. K. Gibson Jr., C. Gonzalez, W. Peabody, Organic matter on the Earth's Moon. *Geochim. Cosmochim. Acta* **134**, 1–15 (2014).

62. A. El Goresy, M. Chen, P. Gillet, L. Dubrovinsky, G. Graup, R. Ahuja, A natural shock-induced dense polymorph of rutile with α-PbO_2 structure in the suevite from the Ries crater in Germany. *Earth Planet. Sci. Lett.* **192**, 485–495 (2001).

63. J. C. Jackson, J. W. Horton Jr., I.-M. Chou, H. E. Belkin, A shock-induced polymorph of anatase and rutile from the Chesapeake Bay impact structure, Virginia, U.S.A. *Am. Mineral.* **91**, 604–608 (2006).

64. J. F. McCone, M. D. Fries, M. Killgore, Raman detection of titania-II, An impact induced rutile polymorph in suevite ejecta at Bosumtwi crater, Ghana. *Lunar Planet. Sci. XXXIX*, Abstract #2450 (2008).

65. M. Chen, X. P. Gu, X. D. Xie, F. Yin, High-pressure polymorph of TiO_2-II from the Xiuyan crater of China. *Chin. Sci. Bull.* **58**, 4655–4662 (2013).

66. B. P. Glass, M. Fries, Micro-Raman spectroscopic study of fine-grained, shock-metamorphosed rock fragments from the Australasian microtektite layer. *Meteoritics Planet. Sci.* **43**, 1487–1496 (2008).

67. F. C. Smith, B. P. Glass, B. M. Simonson, J. P. Smith, A. E. Krull-Davatzes, K. S. Booksh, Shock-metamorphosed rutile grains containing the high-pressure polymorph TiO2-II in four Neoarchean spherule layers. *Geology* **44**, 775–778 (2016).

68. R. Libbey, F. J. Longstaffe, R. Flemming, Clay mineralogy, oxygen isotope geochemistry, and water/rock ratio estimates, Te Mihi area, Wairakei Geothermal Field, New Zealand. *Clays Clay Miner.* **61**, 204–217 (2013).

69. T. M. Ignasiak, L. Kotlyar, F. J. Longstaffe, O. P. Strausz, D. S. Montgomery, Separation and characterization of clay from Athabasca asphaltene. *Fuel* **62**, 353–362 (1983).

70. J. L. McKay, F. J. Longstaffe, Tracking fluid movement during cyclic steam stimulation of clearwater formation oil sands using stable isotope variations of clay minerals. *Clays Clay Miner.* **61**, 440–460 (2013).

71. L. Ferrière, C. Koeberl, W. U. Reimold, Characterisation of ballen quartz and cristobalite in impact breccias: New observations and constraints on ballen formation. *Eur. J. Mineral.* **21**, 203–217 (2009).

72. S. Terashima, M. Taniguchi, M. Mikoshiba, N. Imai, Preparation of two new GSJ geochemical reference materials: Basalt JB-1b and coal fly ash JCFA-1. *Geostand. Geoanal. Res.* **22**, 113–117 (1998).

73. N. Imai, S. Terashima, S. Itoh, A. Ando, 1994 compilation of analytical data for minor and trace elements in seventeen GSJ geochemical reference samples, "Igneous rock series". *Geostand. Geoanal. Res.* **19**, 135–213 (1995).

74. J. Kirschvink, The least-squares line and plane and the analysis of palaeomagnetic data. *Geophys. J. R. Astr. Soc.* **62**, 699–718 (1980).

75. O. Abramov, D. A. Kring, Numerical modeling of an impact-induced hydrothermal system at the Sudbury crater. *J. Geophys. Res.* **109**, 16 (2004).

76. H. Wilhelm, P. Heidinger, J. Šafanda, V. Čermák, H. Burkhardt, Y. Popov, High resolution temperature measurements in the borehole Yaxcopoil-1, Mexico. *Meteorit. Planet. Sci.* **39**, 813–819 (2004).

77. G. R. Osinski, J. G. Spray, P. Lee, Impact-induced hydrothermal activity within the Haughton impact structure, arctic Canada: Generation of a transient, warm, wet oasis. *Meteoritics Planet. Sci.* **36**, 731–745 (2001).

78. G. R. Osinski, P. Lee, J. Parnell, J. G. Spray, M. Baron, A case study of impact-induced hydrothermal activity: The Haughton impact structure, Devon Island, Canadian High Arctic. *Meteoritics Planet. Sci.* **40**, 1859–1877 (2005).

79. R. L. Christiansen, *U.S.G.S. Prof. Paper* **729**-G, 146 (2001).

80. R. O. Fournier, in *Geothermal Biology and Geochemistry in Yellowstone National Park* (Montana State Publications, 2005), pp. 3–29.